Small Structures

small structures

www.small-structures.com

RESEARCH ARTICLE OPEN ACCESS

Fabrication of Transparent Microneedle Patch for Minimally Invasive Glucose Monitoring Optical Biosensor

Nayeon Kwon[1] | Yerin Hong[1] | Daehyeon Yoo[1] | Yongsuk Eo[2] | Seokho Jung[1] | Hoesung Yang[3] | Jinah Lee[4] | Siyun Lee[1] | WonJun Jang[5,6] | Han-Jun Kim[5,6,7] | Dong Nyoung Heo[4,8] | Jinwook Yoon[1] | Il Keun Kwon[8] | Dae Hyeok Yang[9] | Junhong Min[10] | Taek Lee[1]

[1]Department of Chemical Engineering, Kwangwoon University, Seoul, Republic of Korea | [2]AbGTech, Seoul, Republic of Korea | [3]Digital Convergence Research Laboratory, Electronics and Telecommunications Research Institute (ETRI), Daejeon, Republic of Korea | [4]Biofriends Inc., Seoul, Republic of Korea | [5]Interdisciplinary Major Program in Innovative Pharmaceutical Sciences, Korea University, Sejong, Republic of Korea | [6]College of Pharmacy, Korea University, Sejong, Republic of Korea | [7]Department of Plastic and Reconstructive Surgery, College of Medicine, Korea University, Seoul, Republic of Korea | [8]Department of Dental Materials, Kyung Hee University, Seoul, Republic of Korea | [9]Department of Biologics and Engineering, The Catholic University of Korea, Bucheon-si, Gyeonggi-do, Republic of Korea | [10]School of Integrative Engineering, Chung-Ang University, Seoul, Republic of Korea

Correspondence: Dae Hyeok Yang (yangdh@catholic.ac.kr) | Junhong Min (junmin@cau.ac.kr) | Taek Lee (tlee@kw.ac.kr)

Received: 3 February 2026 | **Revised:** 3 April 2026 | **Accepted:** 10 April 2026

Keywords: colorimetric change | glucose | glucose oxidase | microneedle | minimally invasive | nude mice | optical biosensor

ABSTRACT

Diabetes is a growing global health concern that requires continuous glucose monitoring. Conventional methods involve painful blood sampling, which is particularly challenging for young and elderly patients. Microneedle (MN) emerges as minimally invasive devices that enable blood glucose monitoring without pain. However, most reported MN sensors rely on amperometric methods, which reduce biocompatibility due to mediator release and toxicity. To address this, acetic acid and chitosan MN (A.C. MN) were fabricated using biocompatible chitosan and glycerin for mechanical strength. Glucose oxidase (GOx) is incorporated as a probe, enabling glucose detection without additional immobilization. The A.C. MN array (15 × 15, 700 μm length) absorbs ≈5 μL of interstitial fluid in agarose skin models and nude mice. An optical biosensor integrated with a Bluetooth module captures GOx-mediated colorimetric responses and transmits real-time glucose data. Luminosity values increase linearly with glucose concentration, achieving a detection limit of 23.9 mg dL^{-1}. Specificity tests confirm selective glucose detection in interstitial fluid. In vivo evaluation using diabetic and normal mice demonstrates distinct glucose responses, validating device functionality. This minimally invasive A.C. MN biosensor eliminates enzyme immobilization steps, enhances patient comfort, and provides portable real-time monitoring, making it a promising platform for glucose management.

1 | Introduction

Diabetes is a metabolic disorder characterized by chronic hyperglycemia that leads to vascular damage, particularly affecting the intestines, eyes, kidneys, and nerves, ultimately contributing to severe complications [1–4]. According to the International Diabetes Federation (IDF), the number of adult patients with diabetes is expected to reach 643 million by 2030 and 783 million by 2045. The World Health Organization (WHO) established the Global Diabetes Compact [5, 6], and this epidemic is becoming a particularly serious problem in developing countries and aging societies. Despite this severity, there is still no complete cure for diabetes, requiring long-term medication or insulin to maintain physiological homeostasis in patients [7]. Effective diabetes management and therapeutic intervention require a continuous glucose monitoring system rather than intermittent point-of-care measurements [8]. Transient hyperglycemic and hypoglycemic excursions, which critically influence disease progression and acute complications, cannot be adequately captured through

This is an open access article under the terms of the Creative Commons Attribution License, which permits use, distribution and reproduction in any medium, provided the original work is properly cited.

© 2026 The Author(s). *Small Structures* published by Wiley-VCH GmbH.

single-time-point measurements [9, 10]. Self-monitoring of blood glucose (SMBG) remains the most widely adopted approach in diabetes management, providing discrete glucose concentration data through commercial devices such as FreeStyle Libre, Dexcom G7, and Guardian Connect [11]. These conventional systems rely primarily on capillary blood sampling via lancet-based finger pricking [12], imposing inherent limitations including invasiveness, patient discomfort, and reduced compliance during frequent or long-term use.

Microneedle (MN) has emerged as a transformative solution to address these unmet clinical needs by enabling access to interstitial fluid (ISF) through minimally invasive methods [13–15]. ISF has been recognized as a promising surrogate for blood glucose monitoring, reflecting systemic metabolic status with a short time delay through capillary filtration and dynamic material exchange between the vasculature and surrounding cells [16, 17]. Unlike conventional hypodermic needles used in SMBG, MN does not reach the depth of nerves or blood vessels, thereby facilitating painless and bloodless ISF extraction [18–21]. ISF accessed via MN represents an optimal diagnostic medium for biosensor-based glucose detection in diabetes management, offering a practical and patient-friendly alternative to conventional SMBG approaches [22].

Glucose oxidase (GOx) has been established as the gold-standard glucose recognition element due to its high substrate specificity toward β-D-glucose and robust operational stability [23]. As summarized in Table 1, most conventional biosensors for blood glucose monitoring employ amperometric methods that use GOx as the recognition probe. Through successive technological developments, including mediator-assisted electron transfer [36], immobilization strategies [37], and direct electron transfer architectures [38], GOx-based amperometric glucose monitoring systems have achieved substantial clinical success and reliability. Nevertheless, potential leaching of diffusible mediators in implantable environments may raise concerns regarding localized toxicity [39], while the intrinsic reliance on electrode-mediated signal transduction introduces additional architectural complexity. These factors can complicate long-term stability, biocompatibility, and system integration.

Optical biosensing represents an alternative signal transduction paradigm that fundamentally decouples glucose recognition from electrochemical processes by directly converting enzymatic or biochemical reactions into optical outputs—such as colorimetric, fluorescent, or luminescent signals [40–42]. This mediator-free and electrically decoupled architecture inherently mitigates issues associated with mediator leakage, electrode fouling, and electrical interference, thereby enhancing operational stability and safety. Optical readout enables intuitive signal visualization and remote detection using compact photodetectors or smartphone-based imaging systems, facilitating frequent self-monitoring without sophisticated instrumentation [43]. When integrated with MN platforms for ISF access, optical biosensors provide a minimally invasive, user-centric, and biocompatible solution for continuous diabetes monitoring, positioning optical MN-based glucose sensors as a compelling alternative to conventional electrochemical systems.

In this study, we designed a minimally invasive optical glucose monitoring system through an acetic acid and chitosan MN (A.C. MN) patch. Chitosan is a biocompatible and non-toxic polysaccharide containing amino functional groups that readily form gels through acid-mediated reactions [44]. The chitosan-based matrix provides a suitable environment for colorimetric signal transduction without inhibiting GOx activity, owing to its inherent transparency and mild physicochemical properties. By directly integrating GOx into the MN matrix, continuous glucose recognition and signal generation are achieved through the consumptive behavior of the enzyme, whereby GOx-catalyzed glucose oxidation progressively depletes enzymatically active GOx within the MN patch, resulting in a distinct color transition from yellow to transparent without the need for additional enzyme immobilization or electrode interfaces. This visually gradient change is quantitatively measured through an optical readout system, and optical sensing module supports Bluetooth-based wireless data transmission, facilitating real-time monitoring and data acquisition on external devices. A schematic illustration of the proposed glucose monitoring platform is shown in Figure 1.

2 | Results and Discussion

2.1 | Fabrication of the A.C. MN Patch

The A.C. MN patch was fabricated through a mold-based replication process designed to precisely transfer the MN (Figure 2a). The geometric parameters of the master mold were designed to ensure uniform array formation (Figure 2b), and optical microscopy analysis confirmed the accurate realization of the intended MN height and sharp pyramidal profiles (Figures 2c and S1). Polydimethylsiloxane (PDMS) negative mold was subsequently prepared (Figure 2d), faithfully replicating the MN cavities without observable deformation or collapse. The successful transfer of the master mold geometry into the PDMS mold enabled consistent fabrication of the A.C. MN patch. The resulting MN patch exhibited a translucent brown appearance (Figure S2), indicative of uniform polymer formation throughout the array. Scanning electron microscopy (SEM) images revealed that the final MN patch consisted of a highly ordered array of square pyramid-shaped MN with uniform size and spacing across the entire patch area (Figure 2e). Each MN was well-formed with sharp tips and smooth sidewalls, exhibiting an average height of ≈700 μm and a lateral dimension of 300 μm (Figure 2f). This square pyramidal geometry and needle height were intentionally selected to provide sufficient mechanical strength for effective skin penetration while minimizing discomfort and avoiding damage to deeper vascular and neural tissues, thereby enabling minimally invasive access to ISF [18]. To ensure mechanical robustness during handling and application, the MN patch was supported by a backsheet with an average thickness of 0.3 cm, which prevented structural deformation or fracture prior to skin insertion. Based on preliminary sensing experiments, a minimum ISF volume of ≈5 μL was required to achieve reliable glucose quantification. Accordingly, an MN array comprising 225 was fabricated to meet this sampling requirement (Table S1). The fracture force of a single MN was 0.08 N ± 0.01 per needle, exceeding the minimum force required for skin penetration (0.058 N per needle) [45] (Table S2). These results confirm that the fabricated patch possesses sufficient mechanical strength and structural stability for insertion. Assuming a square pyramidal geometry, the internal volume was estimated to be 0.021 μL per MN, resulting

26884062, 2026, 5, Downloaded from https://onlinelibrary.wiley.com/doi/10.1002/sstr.70437 by Chung-Ang Library - Chung-Ang University , Wiley Online Library on [07/06/2026]. See the Terms and Conditions (https://onlinelibrary.wiley.com/terms-and-conditions) on Wiley Online Library for rules of use; OA articles are governed by the applicable Creative Commons License

TABLE 1 | Comparison table of glucose detection MN.

Method	Probe	MN specifications	MN body materials	Detection time	Liner range (LOD)	Reference
Amperometric	GOx	818 ± 35 μm length	Poly (*o*-phenylenediamine)	15 s	0–252.0 mg dL^{-1} (1.8 mg dL^{-1})	[24]
Amperometric	GOx	1000 μm length	Au	15 ± 9 s	0–450.0 mg dL^{-1} (1.8 mg dL^{-1})	[25]
power density	GOx	50 carbon fibers bundle of 3000 μm length	Tetrathiafulvalene/carbon paste	NM	90.0–450.0 mg dL^{-1} (1.8 mg dL^{-1})	[26]
Amperometric	GOx	680 μm length	Poly (3,4-ethylenedioxythiophene)	15 s	36.0–432.0 mg dL^{-1} (NM)	[27]
Amperometric	GOx	Nano-sphere with 300 nm diameter	Polyvinylidene fluoride-Nafion	30 s	0–360.0 mg dL^{-1} (1.8 mg dL^{-1})	[28]
Amperometric	GOx	280 μm diameter	Ferrocene monocarboxylic acid	36 s	36.0–243.0 mg dL^{-1} (ND)	[16]
Amperometric	GOx	700 μm length	Pt	315 s	0–500.0 mg dL^{-1} (50.0 mg dL^{-1})	[29]
Amperometric	Flavin adenine dinucleotide glucose dehydrogenase	Pores with diameters of ≈25 μm	6-(ferrocenyl)hexanethiol/highly porous gold	3 s	1.8–180.0 mg dL^{-1} (ND)	[30]
Amperometric	GOx-attached polyterthiophene carboxylic acid	700 μm length	Au	10 s	0.9–360.0 mg dL^{-1} (4.0 mg dl^{-1})	[31]
Amperometric	GOx	500 μm length	Overoxidized polypyrrole/gold nanoparticles/Nafion.	28 s	0–46.8 mg dL^{-1} (0.7 mg dL^{-1})	[32]
Amperometric	GOx	800 μm length	Silk/polyols	26 s	30.6–187.2 mg dL^{-1} (ND)	[33]
Amperometric	GOx	500 μm length	Au	1 min	54.0–432.0 mg dL^{-1} (0.9 mg dL^{-1})	[34]
Optical	GF-monomer	650 μm length	Silk fibroin/Polyvinyl Alcohol	20 min	50.0–450.0 mg dL^{-1} (ND)	[35]
Optical	GOx	700 μm length	Acetic acid/Chitosan	20 min	100–500 mg dL^{-1} (23.9 mg dL^{-1})	This study

Note: ND means not determined.

26884062, 2026, 5, Downloaded from https://onlinelibrary.wiley.com/doi/10.1002/sstr.70437 by Chung-Ang Library - Chung-Ang University , Wiley Online Library on [07/06/2026]. See the Terms and Conditions (https://onlinelibrary.wiley.com/terms-and-conditions) on Wiley Online Library for rules of use; OA articles are governed by the applicable Creative Commons License

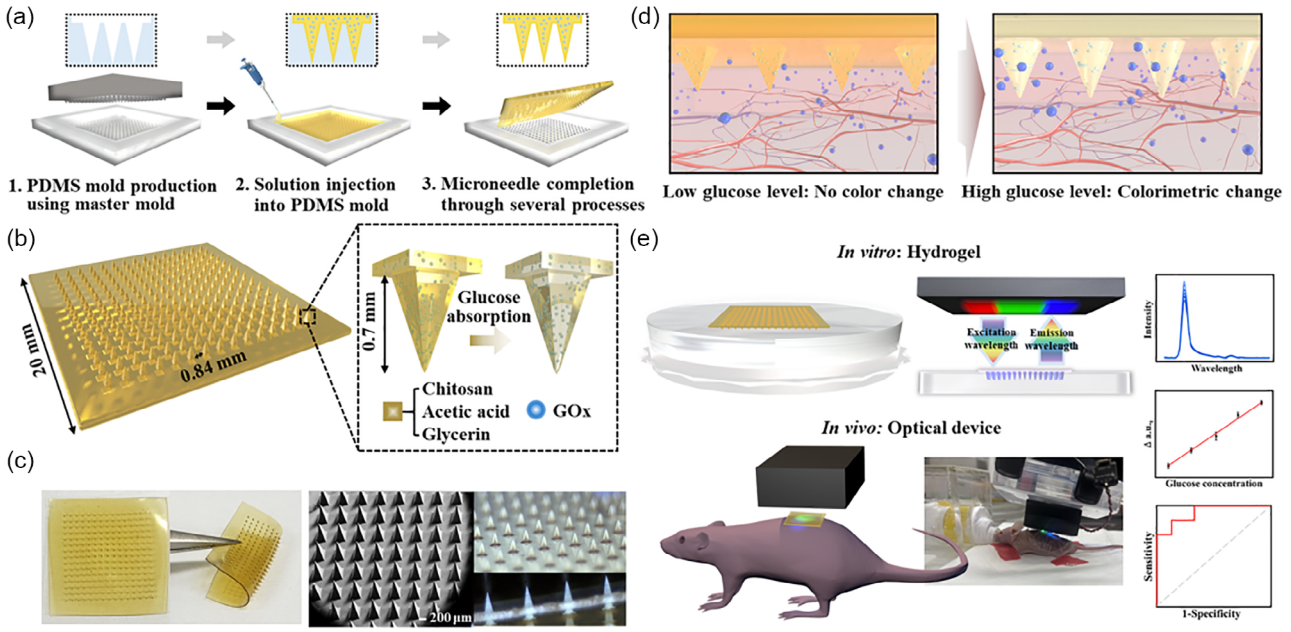


FIGURE 1 | Schematic illustration of the optical glucose-monitoring system through an A.C. MN patch. (a) Stamping-based fabrication process and (b) structural characteristics of the A.C. MN patch. (c) Optical and microscopic images of the fabricated A.C. MN patch. (d) Colorimetric sensing mechanism and (e) application of the A.C. MN patch for glucose detection.

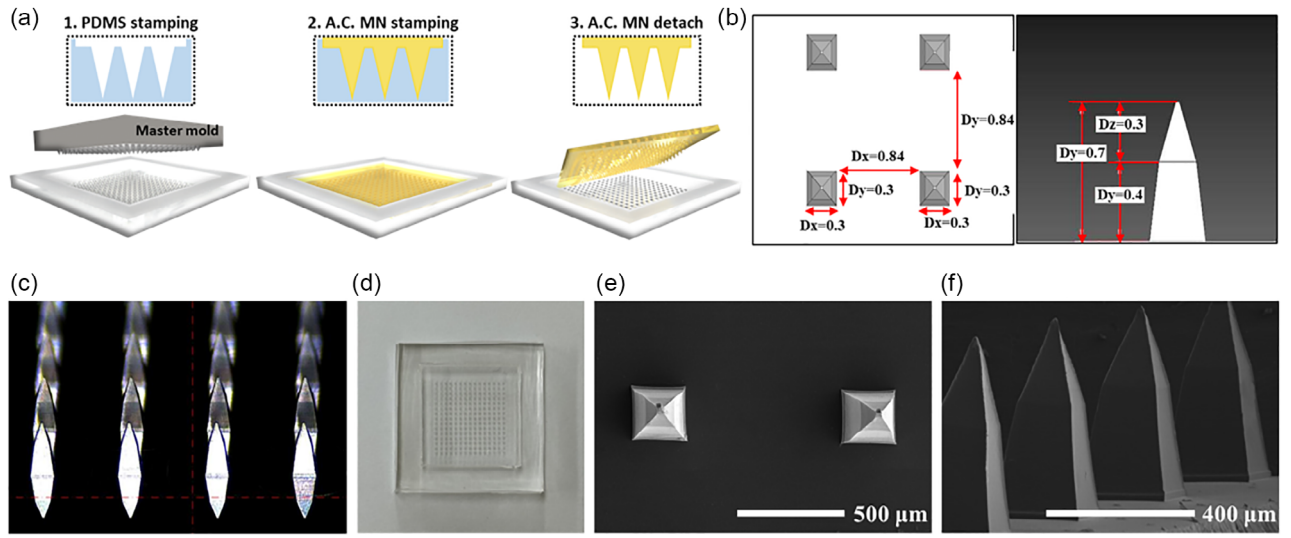


FIGURE 2 | (a) Schematic illustration of the stepwise A.C. MN patch fabrication process. (b) Geometric design parameters of the master mold array. (c) Optical microscopy images of the master mold side-view geometry. (d) Photography image of PDMS mold. (e) SEM images of the MN array taken from above showing the size, spacing of the MN, and the designed pyramidal MN structure. (f) SEM image showing the height of the uniform and well-formed MN.

in a total volume of 4.725 μL for the A.C. MN patch. When a swelling ratio of 20%, obtained from agarose gel experiments, was applied, the effective ISF absorption capacity per MN increased to ≈5.67 μL. Furthermore, considering physiological ISF turnover dynamics—where ISF is continuously exchanged and drained through the lymphatic system at reported rates of ≈0.1–0.2 μL min^{-1} mm^{-2}—an ISF flux of ≈0.6–1.2 mL h^{-1} was estimated over an area of 1 cm^2. Collectively, these results indicate that the designed A. C. MN patch configuration provides sufficient and continuous ISF availability to support reliable glucose sensing.

2.2 | Performance Evaluation of the A.C. MN Biosensor

The performance of the A.C. MN patch as a glucose biosensor was evaluated using a 2% agarose-based skin-mimicking in vitro model containing controlled glucose concentrations (Figures 3a and S3) [46]. The platform was designed to detect glucose-induced colorimetric changes within the MN patch through a reflectance-based optical sensing strategy. The loading efficiency of GOx within the A.C. MN patch was quantified using an activity-based assay, revealing that 94.2 ± 19.5% of the enzyme was successfully incorporated in an active form (Figure S4).

26884062, 2026, 5, Downloaded from https://onlinelibrary.wiley.com/doi/10.1002/sstr.70437 by Chung-Ang Library - Chung-Ang University , Wiley Online Library on [07/06/2026]. See the Terms and Conditions (https://onlinelibrary.wiley.com/terms-and-conditions) on Wiley Online Library for rules of use; OA articles are governed by the applicable Creative Commons License

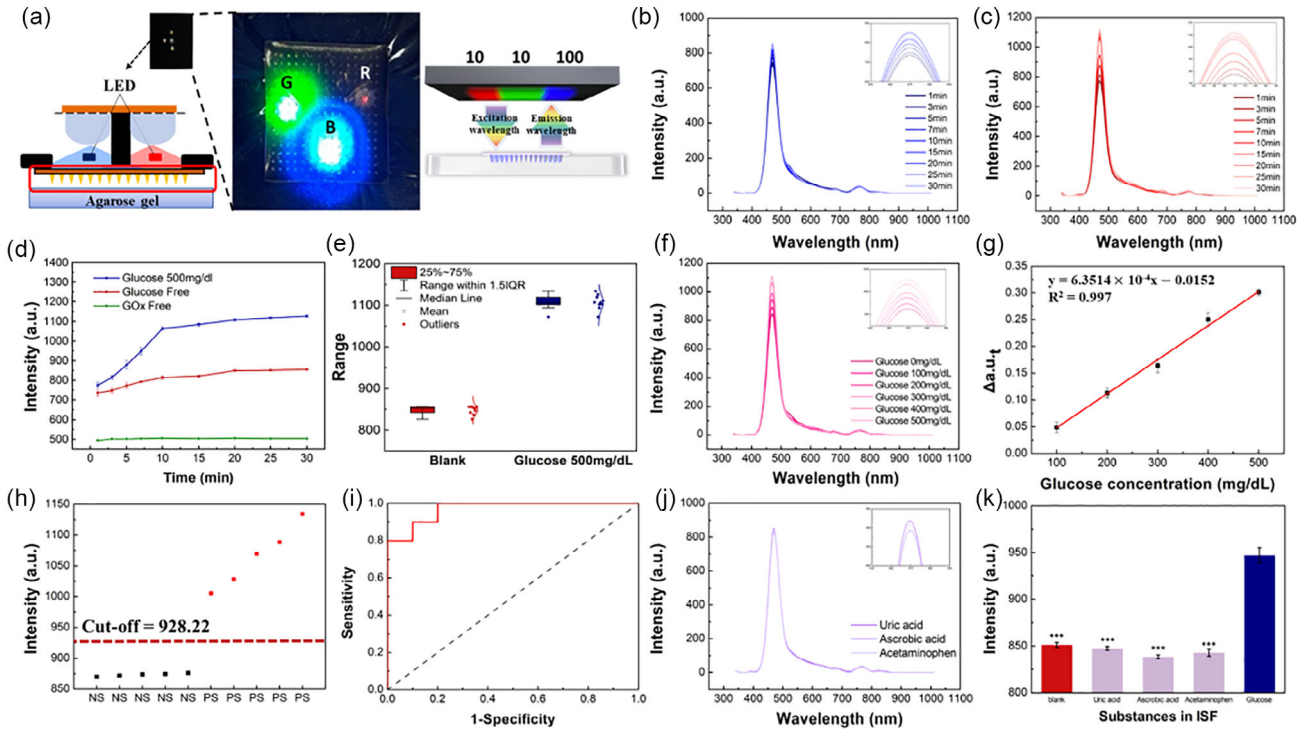


FIGURE 3 | (a) Schematic illustration of the fabricated optical MN biosensing system. Time-dependent colorimetric response of the A.C. MN biosensor for the (b) blank sample and (c) 500 mg dL^{-1} glucose. (d) Peak intensity comparing results of the time-dependent brightness for the blank and 500 mg dL^{-1} glucose. (e) Box plot representing the detection time for the blank and 500 mg dL^{-1} Glucose. (f) Colorimetric response of the A.C. MN biosensor for various glucose concentrations (0 to 500 mg dL^{-1}). (g) Calibration curve by $\Delta a.u._t$ values according to Glucose concentration. (h) False-positive test to demonstrate clinical applicability of sensor: a.u. peak values for the bottom five of NS and top five of PS results. (i) Receiver operating characteristic curve for classification of diabetic patients. (AUC: 0.970, Asymptotic 95% confidence interval: 0.907–1.000). (j) Colorimetric response of Uric acid, Ascorbic acid, and Acetaminophen. (k) Selective reactivity test of the A.C. MN biosensor against non-target substances contained in ISF. All measurements were performed with ten replicates ($n = 10$).

Among the RGB channels, the blue wavelength region exhibits the highest sensitivity to changes in chromophore absorption associated with the yellow to transparent transition, and the blue channel was assigned a dominant weighting (100), while the red and green channels were maintained at lower auxiliary levels (10) (Figure S5). The reflected intensity signal was wirelessly transmitted to a personal computer via Bluetooth Low Energy (BLE), resulting in a real-time detection signal.

Applied to an agarose skin model without glucose (blank), there was minimal wavelength change, and the peak value remained relatively constant, indicating that GOx remained inactive due to the absence of glucose. The increase in the signal intensity value to 854.764 arbitrary units (a.u.) was attributed to water absorption from agarose, which caused the patch to swell and become more transparent (Figure 3b). In contrast, when the patch was applied to an agarose model containing glucose, the signal increased steadily at 1, 3, 5, 7, and 10 min, reaching 1108.019 a.u. at 20 min (Figure 3c). This tendency was also observed in the blank sample. Beyond this point, the standard error decreased, and the signal stabilized at a nearly constant value. Whereas, the GOx-free control exhibited a lower signal intensity with minimal temporal variation (Figure 3d). These results indicate that the optical signal arises from a combined effect of swelling and enzyme-induced modulation of the patch microenvironment matrix. Box plot analysis further demonstrated the reproducibility of the A.C. MN biosensor in terms of detection time (Figure 3e). In addition, the A.C. MN patch did not dissolve or disintegrate after reacting with glucose, and while swelling occurred, the MN remained intact (Figure S6). This indicates that the A.C. MN biosensor retained its structural integrity and was capable of effectively extracting ISF after glucose detection.

At various glucose concentrations in the agarose skin model, higher glucose levels promoted GOx-catalyzed oxidation reactions, consuming GOx within the patch and generating intensified colorimetric signals with correspondingly higher peak values. To assess sensor sensitivity, a calibration curve was plotted using the following Equation (1):

$$\Delta\,a.u._t = \frac{(a.u._t - a.u._{blank})}{a.u._{blank}} \quad (1)$$

where $a.u._t$ represents the peak signal value when the biosensor reacts with glucose at each concentration, and $a.u._{blank}$ is the peak signal value of the blank sample.

The normalized signal exhibited a linear correlation with glucose concentration over the range of 100–500 mg dL^{-1} (Figure 3f). The calibration curve displayed a slope of 6.3514×10^{-4} and a y-intercept of −0.0152, with excellent linearity ($R^2 = 0.997$) (Figure 3g). The limit of detection (LOD) was calculated using Equation (2):

26884062, 2026, 5, Downloaded from https://onlinelibrary.wiley.com/doi/10.1002/sstr.70437 by Chung-Ang Library - Chung-Ang University , Wiley Online Library on [07/06/2026]. See the Terms and Conditions (https://onlinelibrary.wiley.com/terms-and-conditions) on Wiley Online Library for rules of use; OA articles are governed by the applicable Creative Commons License

$$y_{dl} = y_{blank} + 3.3SD \quad (2)$$

where y_{dl} is the signal value at the detection limit, y_{blank} is the average signal value of the blank, and SD is the standard deviation; the calculated LOD was 23.9 mg dL^{-1}. These results indicate that the A.C. MN patch can sensitively detect glucose within the physiological range by monitoring the peak signal changes resulting from colorimetric variations.

To assess the field applicability of the proposed A.C. MN biosensing platform, positive (PS) and negative (NS) samples were tested. The criteria for distinguishing NS from PS samples were based on the IDF and WHO guidelines, setting a standard of 126 mg dL^{-1} as the random glucose concentration in patients with diabetes measured 12 h after fasting [47]. Accordingly, the PS samples were simulated by preparing an agarose skin model with a random glucose concentration within the linear range of the calibration curve at 126 mg dL^{-1} or higher. For the NS samples, reflecting the normal random blood glucose range of 126 mg dL^{-1} or less in the general population, an agarose skin model was prepared with a glucose concentration between these values. A comparison of the peak a.u. values between the top five PS ($n = 10$) and the bottom five NS ($n = 10$) samples are presented (Figure 3h). The NS values showed minimal variation, whereas the PS values displayed a much broader distribution. Analysis of all samples revealed that the signal value range for NS was 69.069 a.u., whereas it was 220.772 a.u. for PS. These data show that the distribution range of PS samples is wider than that of NS samples and that the signal value of the sensor is sensitive to the concentration. Thus, receiving operator characteristic (ROC) curve analysis was used to enhance the accuracy of the sensor performance evaluation. Diagnostic performance was evaluated by plotting the sensitivity against 1-specificity on the ROC curve. The accuracy of the sensor was evaluated by calculating the area under the ROC curve (AUC). It was confirmed that the sensor had high accuracy, with an AUC value of 0.970, close to the maximum value of 1. The cut-off value of A.C. MN to detect positive and negative results for the discrimination of patients with diabetes was selected as 928.222 a.u., where the sensitivity and specificity were both 90% (Figure 3i).

2.3 | Verification of the Capability of the A.C. MN Biosensor to Detect ISF

The detection performance of the A.C. MN biosensor can be influenced by the interference from electrolytes and metabolites present in the ISF [48]. To evaluate the response of the biosensor to such interference, uric acid, ascorbic acid, and acetaminophen, which are common exogenous interferents in the blood and ISF, were tested. According to the ISO 15 197 guidelines, the concentrations were set at 23.5 mg dL^{-1} for uric acid, 3 mg dL^{-1} for ascorbic acid, and 4 mg dL^{-1} for acetaminophen, reflecting the typical levels found in the serum [49, 50]. These conditions were used to assess the specificity of the sensor for detecting glucose within the ISF. After adding the interferents to the agarose skin model at the specified concentrations, the A.C. MN biosensor patch was applied and allowed to react for 20 min, similar to the glucose testing protocol (Figure 3j). A comparison of the peak signal values for each interfering substance revealed negligible differences from the blank signal. According to the IDF, WHO, and American Diabetes Association, diabetes is diagnosed when one or more of the following criteria are met: fasting plasma glucose ≥126 mg/dL, plasma glucose ≥200 mg/dL 2 h after a 75 g oral glucose load, or random plasma glucose >200 mg/dL [51, 52]. Compared to the glucose response at 200 mg dL^{-1}, a level indicative of diabetes according to the IDF and WHO criteria, the response to interfering substances was minimal. This indicates that the A.C. MN glucose sensor can accurately detect the glucose levels in ISF without interference from other substances (Figure 3k).

2.4 | Blood Glucose Monitoring With A.C. MN Biosensor in Nude Mice

The feasibility of the A.C. MN biosensor was verified in nude mice (Figures 4a and S7) [53]. Prior to measurement, the mice were fasted for 12 h to assess diabetic status based on fasting blood glucose levels. Blood glucose levels were first measured using a commercial glucose meter before applying the A.C. MN patch, allowing confirmation of the baseline glucose levels in both normal and diabetic nude mice. The A.C. MN patch, minimally invasively applied to the skin, underwent a colorimetric change over a 40 min period, which was monitored using an optical device. In diabetic mice, the signal value at the detection time reached 773.538 a.u., indicating a strong response due to the elevated glucose concentration. In contrast, normal mice exhibited a lower signal value of 520.062 a.u. with relatively little increase (Figure 4b). These trends were consistent with those observed in the agarose skin model, and higher glucose concentrations also led to more pronounced signal increases. The MN pierced the skin and properly absorbed the interstitial fluid through the pattern formed on the skin after A.C. MN were removed (Figure 4c).

To confirm the actual effect of the A.C. MN biosensor on the epidermis layer of the skin, we applied the MN biosensor to nude mice, collected the skin, and performed histopathological analysis. As can be seen in Figure 4d,e, H&E analysis revealed that the skin treated with the A.C. MN biosensor exhibited a pattern where the epidermis at the MN application sites was indented toward the dermis at regular intervals, resembling the needle arrangement pattern of the A.C. MN patch. At high magnification (10×), the epidermis appeared thinner or partially disconnected at the MN application sites compared to the surrounding epidermis. However, no damage to the entire dermis layer or signs of hemorrhage were observed. These results suggest that the A.C. MN biosensor could successfully cause temporary disconnection of the epidermis, potentially enabling absorption of interstitial fluid from the dermal layer of the skin. Through these, the A.C. MN biosensing platform demonstrates strong potential as a minimally invasive and wearable diagnostic system for continuous glucose monitoring, leveraging optical readout and interstitial fluid access without the need for electrical interfaces or blood sampling. Furthermore, the in vivo performance of the system was validated by comparison with a commercially available glucometer (green doctor, GC Green Cross MS) (Figure 4f). Despite the fundamental difference in measurement modality—where the commercial device provides discrete endpoint measurements while the proposed A.C. MN patch enables continuous monitoring under a single attachment—the two systems exhibited a strong correlation ($R^2 = 0.967$). This agreement demonstrates that the proposed platform can reliably track dynamic glucose fluctuations in vivo, rather than relying on a single reaction endpoint.

26884062, 2026, 5, Downloaded from https://onlinelibrary.wiley.com/doi/10.1002/sstr.70437 by Chung-Ang Library - Chung-Ang University , Wiley Online Library on [07/06/2026]. See the Terms and Conditions (https://onlinelibrary.wiley.com/terms-and-conditions) on Wiley Online Library for rules of use; OA articles are governed by the applicable Creative Commons License

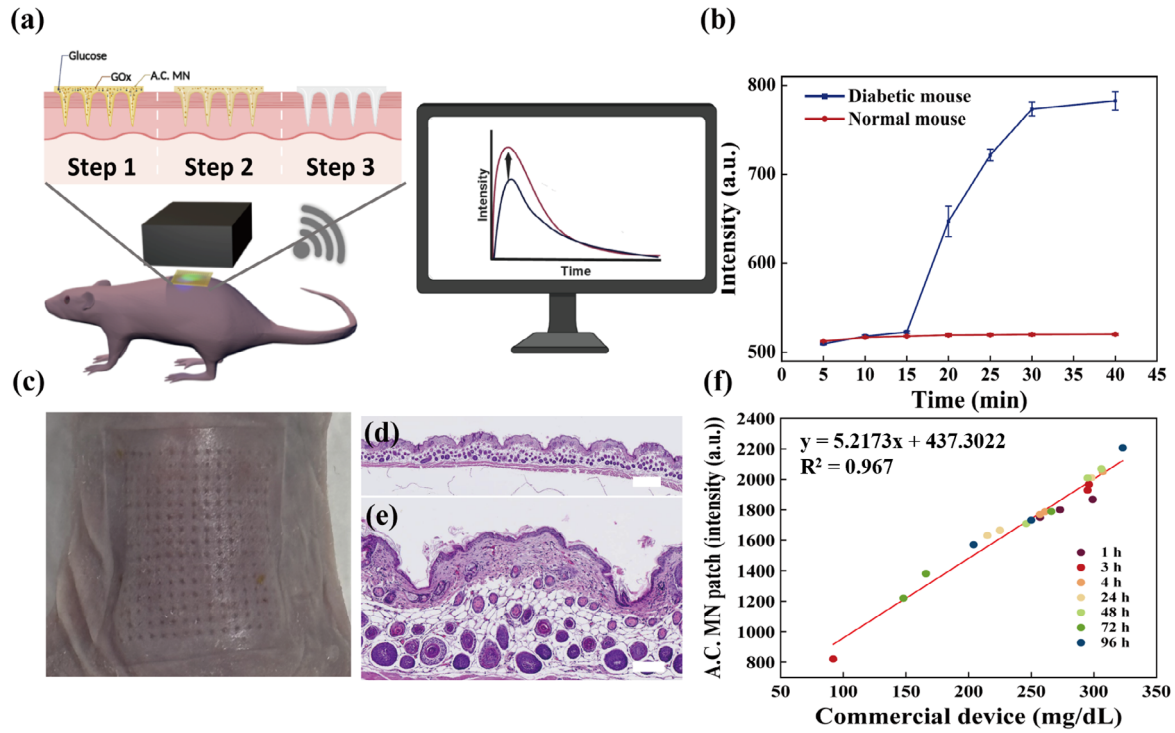


FIGURE 4 | In vivo tests of the A.C. MN biosensor for minimally invasive glucose monitoring. (a) Schematic illustration of the stepwise operation of the A.C. MN biosensor, Step 1: A.C. MN patch insertion into the skin, Step 2: enzymatic glucose reaction within the MN patch, and Step 3: optical signal acquisition using an external detection module with wireless data transmission. (b) Comparison of optical signal values ($n = 10$) of nude mice. The red line and the blue line represent diabetic mouse and normal mouse, respectively. (c) Photograph of the back of a mouse with the patch removed after measurement. (d,e) H&E-stained images of the same skin section after MN application were acquired at 2× and 10× magnifications, respectively. Low magnification (2×) H&E-stained image showing overall skin morphology following MN application. High magnification (10×) view of the same region, highlighting periodic epidermal indentations corresponding to the microneedle array, confirming the minimally invasive nature of the MN-based sensing platform. Scale bars for 2x and 10x show 500 and 100 μm, respectively. (f) Correlation between the signal obtained from the A.C. MN patch and the glucose values measured by a commercial glucometer ($n = 3$).

3 | Conclusion

In this study, an A. C. MN biosensor was developed to address the challenges of conventional glucose monitoring in patients with diabetes. This biosensor was designed to detect blood glucose in the ISF in a minimally invasive manner without causing bleeding or pain. The biosensor was fabricated as an A.C. MN patch by incorporating GOx into the formulation to prevent enzyme loss during immobilization. Glucose detection was achieved by monitoring colorimetric changes using a portable optical device equipped with Bluetooth functionality for real-time measurements in a practical setting. The device demonstrated a sensitive linear response within the physiological range and successfully detected glucose concentrations as low as 23.900 mg dL^{-1}. Reactivity tests confirmed that the A.C. MN biosensor was unaffected by interfering substances in the ISF, ensuring accurate glucose detection. It was verified that it can detect glucose in nude mice. The signal value increased significantly in diabetic mice, and there was almost no change in the signal value in normal mice. This showed a similar tendency as in the agarose skin model, showing that the fabricated biosensor worked properly in actual clinical experiments. Collectively, these results confirm that the A.C. MN biosensor offers a low-cost, high-sensitivity, and painless glucose monitoring solution for patients with diabetes, with the potential to be widely adopted as a portable, wearable patch for continuous glucose monitoring.

4 | Experimental Section

4.1 | Materials

High-molecular-weight chitosan (50–100 kDa) was purchased from Yunzhou Biochemistry (Qingdao, China). Glacial acetic acid and glycerin were obtained from Deoksan Integrated Science (Seoul, South Korea). D-(+)-glucose and glucose oxidase from An GOx were sourced from Sigma–Aldrich (MO, USA). The silicone elastomer base and curing agent used for mold fabrication were acquired from Vision Lab Science (Incheon, South Korea). Horseradish peroxidase (HRP) and 3,3′,5,5′-tetramethylbenzidine were purchased from Sigma–Aldrich (Saint Louis, MO, USA). Agarose for skin model fabrication, which was used in experiments to verify the GOx-glucose reaction in the fabricated patch, was obtained from Hanlab (Seoul, South Korea).

4.2 | Master Mold Design and PDMS Mold Fabrication

The master mold was fabricated using KBIOHEALTH (Cheongju, Korea) from aluminum 6061-T6, with the following dimensions: 2.5 cm in length, 2.5 cm in width, and 0.5 cm in height. The mold contained a 15 × 15 array of MNs, totaling 225 needles, with an inter-needle spacing of 840 μm. Each MN had a square pyramidal shape, measuring 700 μm in height

26884062, 2026, 5, Downloaded from https://onlinelibrary.wiley.com/doi/10.1002/sstr.70437 by Chung-Ang Library - Chung-Ang University , Wiley Online Library on [07/06/2026]. See the Terms and Conditions (https://onlinelibrary.wiley.com/terms-and-conditions) on Wiley Online Library for rules of use; OA articles are governed by the applicable Creative Commons License

and 300 μm per side. A PDMS mold was created using the master mold as a template to fabricate the A.C. MN patch. This mold was prepared by mixing the silicone elastomer base and curing agent in a 10:1 ratio and pouring the mixture over the master mold in a 50 mm × 15 mm petri dish. The setup was placed in a desiccator for 30 min to eliminate air bubbles, followed by curing in an oven at 80°C for 1 h.

4.3 | Optimization of the A.C. MN Patch Composition

The MN comprised acetic acid (wt%), glycerin (wt%), chitosan (wt%), and GOx (mg dl^{-1}). With the chitosan concentration fixed at 5 wt%, solutions were prepared by adjusting the acetic acid concentration to 1, 2, 3, 4, and 5 wt% and the glycerin concentration to 0 and 1 wt%. At an acetic acid concentration of 1 wt%, chitosan did not fully dissolve and remained in powder form. At an acetic acid concentration of 2 wt%, the complete dissolution of chitosan took 24 h, significantly longer than the 3 h dissolution time observed with the other tested concentrations. For acetic acid concentrations of 4 and 5 wt%, the resulting pH was below 4.0, raising concerns about the high acidity that could inhibit GOx activity. Hence, an acetic acid concentration of 3 wt% was selected for further experiments. However, at 3 wt% acetic acid, the pH of the solution remained approximately within the 4.0 range. To ensure a stable pH of 4.2 or higher and a dissolution time of 3 h, the chitosan concentration was increased to 6 wt%. The MN produced with solutions containing 0 wt% glycerin were hard, inflexible, and prone to breakage. In contrast, those made with 1 wt% glycerin demonstrated flexibility, although additional adjustments were deemed necessary. Subsequent experiments were then performed with glycerin concentrations of 1.5, 1.6, 1.7, and 2.0 wt%; 1.6 wt% was identified as the optimal concentration. Hence, the optimal composition for the A.C. MN patch was determined to be acetic acid at 3 wt%, glycerin at 1.6 wt% glycerin, 6 wt% chitosan, and 3 mg dl^{-1} GOx (Table S3).

4.4 | Fabrication of A.C. MN Patch

The fabrication process of the A.C. MN patch consisted of two main steps: solution preparation process and the patch manufacturing. During solution preparation, deionized water and 1.6 wt% glycerin were mixed, and 6 wt% chitosan powder form was added. The mixture was then stirred at 400 rpm using a magnetic stirrer. This step is necessary to prevent the crosslinking reaction between chitosan and acetic acid from causing localized agglomeration, which occurs when acetic acid is added without the proper dispersion of chitosan [54, 55]. Once the chitosan was evenly distributed, the stirring speed was reduced to 150 rpm, and 3 wt% acetic acid was slowly added dropwise, allowing the viscosity of the solution to increase gradually. The solution was then stirred for 3 h to ensure complete mixing. When the solution became transparent, 5 mg dL^{-1} of GOx was added, and the mixture was stirred at 150 rpm for another 3 h to facilitate interactions between the solution and glucose. The loading efficiency of GOx within the A.C. MN patch was quantified using an activity-based HRP–TMB colorimetric assay. Briefly, HRP (0.05 μg mL^{-1}) and glucose (200 mg dL^{-1}) were mixed with the MN-derived GOx solution, and the reaction was incubated at room temperature for 10 min to allow enzymatic generation of hydrogen peroxide. Subsequently, TMB substrate was introduced and allowed to react for 2 min, followed by terminated with 1 M H_2SO_4. The absorbance was measured at 450 nm. The loading efficiency was calculated by comparing the enzymatic activity of the MN-derived GOx with that of the initial GOx solution. The mechanical strength of microneedles was measured by applying a compressive load through a universal testing machine (Roell Z0.5, Zwick Roell, Ulm, Germany). The crosshead speed was 50 μm min^{-1} and the fracture force of a single microneedle was determined from the first inflection point of the force–displacement curve, which represents the onset of structural failure. In contrast, the mechanical robustness of the entire microneedle array was evaluated by recording the compressive load at a predefined displacement of 350 μm, corresponding to the representative insertion depth in skin.

4.5 | In Vitro Environment Setup

To verify the glucose detection capability of the A.C. MN as a biosensor, an in vitro system was designed. Given that the target glucose in this study was located within the ISF beneath the skin, a direct-contact solution environment for the MN would not accurately reflect in vivo conditions. Therefore, an agarose hydrogel, simulating the dermis containing ISF, was developed as a skin model to better predict the in vivo performance of the A.C. MN patch [56]. The hydrogel was prepared by incorporating glucose, uric acid, ascorbic acid, and acetaminophen at target concentrations in 2% agarose. To further replicate the moisture characteristics of the skin, the agarose hydrogel was dried on a clean bench for 24 h to reduce its moisture content. This skin model proved suitable for in vitro testing because no significant deformation of the hydrogel occurred except for minor swelling at the needle contact points when the A.C. MN patch was removed.

4.6 | Optical Device Fabrication and Measurement Specifications

The optical measurement device was designed to monitor colorimetric changes in the A.C. MN patches by irradiating them with a light-emitting diode (LED) light source at specific wavelengths and measuring the reflected light. The device had a rectangular shape, measuring 3.5 cm in height and 4 cm in width. Three LED light sources were used, each with a diameter of 3 Φ and wavelengths of 460 nm ± α, 530 nm ± α, and 770 nm ± α. The light detection unit utilized a semiconductor digital spectrometer sensor capable of detecting energy in the wavelength range of 340–1010 nm to measure colorimetric changes and the a.u. values were defined as the normalized reflected intensity derived from the RGB-based spectral response within the measured range, where the minimum and maximum signals were set using the transparent and white patch states, respectively, to quantify the glucose-induced color transition. Additionally, a Nordic nRF-52 series microprocessor with BLE functionality was employed to control both the light emission and detection units and to transmit data. The wavelength data related to colorimetric

26884062, 2026, 5, Downloaded from https://onlinelibrary.wiley.com/doi/10.1002/sstr.70437 by Chung-Ang Library - Chung-Ang University , Wiley Online Library on [07/06/2026]. See the Terms and Conditions (https://onlinelibrary.wiley.com/terms-and-conditions) on Wiley Online Library for rules of use; OA articles are governed by the applicable Creative Commons License

changes in the A.C. MN patches were stored in the graphical user interface of the PC via BLE communication.

4.7 | Colorimetric Change in Response to Glucose

GOx catalyzes the oxidation of glucose to gluconolactone and hydrogen peroxide, as outlined in the following reactions:

$$\text{Glucose} + \text{GOx}(\text{FAD}) \rightarrow \text{Glucono} - \delta - \text{lactone}$$

$$\text{GOx}(\text{FADH}_2) + \text{O}_2 \rightarrow \text{GOx}(\text{FAD}) + \text{H}_2\text{O}_2$$

The fabricated A.C. MN patches contained GOx, which oxidized glucose upon contact. During this process, the GOx in the patch was consumed, reducing its concentration. Consequently, the initial amount of yellow GOx decreases, causing the patch to change color from yellow to transparent (Figure S5a,b). The A.C. MN patch utilizes chitosan as a medium to visualize the color change in GOx, facilitating glucose detection through these colorimetric changes.

4.8 | In Vivo Test

BALB/c nude mice (male, 7 weeks old, average weight 20–22 g) were purchased from Orientbio (Seoul, South Korea) and maintained under specific pathogen-free conditions (22 ± 2°C, 55 ± 5% humidity, 12 h light/dark cycle) with ad libitum access to standard chow and water. All animal studies were conducted in accordance with the guidelines of the IACUC of Korea University (Approval number: KUIACUC-2025-0055). For the glucose testing, the animals were divided into two groups: a normal control group and a streptozotocin (STZ)-induced diabetic group. Diabetes was induced via a single intraperitoneal injection of STZ (50 mg kg^{-1} body weight) dissolved in citrate buffer (pH 4.5). Mice with fasting blood glucose levels ≥250 mg dL^{-1} were considered diabetic. For in vivo A.C. MN insertion and glucose monitoring, anesthesia was induced and maintained via inhalation of isoflurane (Hana Pharm Co., Ltd., Seoul, South Korea). Isoflurane was administered using a rodent inhalation anesthesia system (Model: JD-C-107A, Jeongdo Bio & Plant Co., Ltd., Seoul, South Korea), which consists of a transparent chamber, flow meters (Dwyer Air cc/min and Air × 100), and a timer-integrated power control switch to ensure stable anesthetic delivery and animal safety. The A.C. MN patches were applied to the dorsal skin of anesthetized mice to enable interstitial fluid extraction and glucose sensing. At the end of the experiments, all animals were humanely euthanized under deep inhalation anesthesia.

4.9 | Measurement of A.C. MN Biosensor in Nude Mice

Minimally invasive A.C. MN biosensor measurements were performed in nude mice. A.C. MN biosensor measurements were performed in three healthy nude mice and three diabetic nude mice. Diabetic mice were prepared by intraperitoneal administration of low-dose STZ to normal mouse repeatedly. STZ was dissolved in 50 mM sodium citrate buffer (pH 4.5) immediately before injection to a final concentration of 4 mg mL^{-1}. Normal mice were administered 40 mg kg^{-1} STZ for five consecutive days, and diabetic mice were prepared by feeding 10% sucrose water instead of regular water. Blood glucose concentrations of prepared healthy nude mouse and diabetic nude mouse were analyzed from tail vein blood samples, and diabetes was confirmed by measuring glucose using a glucometer (green doctor, GC Green Cross MS, South Korea). A.C. MN patches were fixed to the back of mouse using 3 M Tegaderm film. For optical measurements via the device, mice were anesthetized during the measurements.

4.10 | Histopathological Evaluation

Neutralized buffered formalin-fixed skin samples were trimmed and then dehydrated and paraffin-embedded using standard tissue processing methods. Paraffin blocks were sectioned into 4–5 μm thick slides using a microtome, followed by deparaffinization/rehydration and hematoxylin and eosin (HE) staining. All HE-stained slides were scanned as whole slide scans with a Motic EasyScan One FL slide scanner (Motic, China).

4.11 | Statistical Analysis

Standard and balanced errors were calculated for each dataset and analyzed using SPSS (Version 19.0, IBM Corp., New York). Significant differences were assessed by one-way analysis of variance (ANOVA) with equal variances using the Tukey and LSD algorithms for cross-validation. A probability value was marked as *** $p < 0.001$, indicating significant differences.

Acknowledgements

This work was supported by the National Research Foundation of Korea (NRF) grant funded by the Korea government (MSIT) (RS-2026-25473418) and by the National Research Foundation of Korea (NRF) grant funded by the Korea government (MSIT) (RS-2024-00416117) and by the Materials & Components Technology Development Program (RS-2024-00507931, The development of multiplex array diagnostic materials and pretreatment modules for analyzing inflammatory diseases in the elderly) funded By the Ministry of Trade Industry & Energy (MOTIE, Korea) and by Ministry of Trade, Industry and Energy (MOTIE) (RS-2023-KT226565).

Funding

This study was supported by National Research Foundation of Korea (NRF) (RS-2026-25473418, RS-2024-00416117), Materials & Components Technology Development Program (RS-2024-00507931), Ministry of Trade, Industry and Energy (MOTIE) (RS-2023-KT226565).

Conflicts of Interest

The authors declare no conflicts of interest.

Data Availability Statement

The data that support the findings of this study are available from the corresponding author upon reasonable request.

References

1. Y. Li, Y. Liu, S. Liu, et al., "Diabetic Vascular Diseases: Molecular Mechanisms and Therapeutic Strategies," *Signal Transduction and Targeted Therapy* 8, no. 1 (2023): 152, https://doi.org/10.1038/s41392-023-01400-z.

26884062, 2026, 5, Downloaded from https://onlinelibrary.wiley.com/doi/10.1002/sstr.70437 by Chung-Ang Library - Chung-Ang University , Wiley Online Library on [07/05/2026]. See the Terms and Conditions (https://onlinelibrary.wiley.com/terms-and-conditions) on Wiley Online Library for rules of use; OA articles are governed by the applicable Creative Commons License

2. X. Lu, Q. Xie, X. Pan, et al., "Type 2 Diabetes Mellitus in Adults: Pathogenesis, Prevention and Therapy," *Signal Transduction and Targeted Therapy* 9, no. 1 (2024): 262, https://doi.org/10.1038/s41392-024-01951-9.

3. M. Z. Banday, A. S. Sameer, and S. Nissar, "Pathophysiology of Diabetes: An Overview," *Avicenna Journal of Medicine* 10 (2020): 174–183, https://doi.org/10.4103/ajm.ajm_53_20.

4. K. D. Barnard-Kelly and R. I. Holt, "The Aims of Diabetes Care," in *Textbook of Diabetes* (Wiley, 2024), 341–353.

5. H. Sun, P. Saeedi, S. Karuranga, et al., "Global Epidemiology of Diabetes," *Diabetes Research and Clinical Practice* 183 (2022): 109119, https://doi.org/10.1016/j.diabres.2021.109119.

6. E. W. Gregg, J. Buckley, M. K. Ali, et al., "Improving Health Outcomes of People with Diabetes: Target Setting for the WHO Global Diabetes Compact," *The Lancet* 401, no. 10384 (2023): 1302–1312, https://doi.org/10.1016/S0140-6736(23)00001-6.

7. L. Starr, S. Dutta, T. Danne, S. R. Karpen, C. Hutton, and A. Kowalski, "The Urgent Need for Breakthrough Therapies and a World without type 1 Diabetes," *Diabetes Therapy* 16, no. 6 (2025): 1063–1076, https://doi.org/10.1007/s13300-025-01735-.

8. I. B. Hirsch, S. K. Garg, E. Repetto, et al., "Continuous Glucose Monitoring Frequency and Glycemic Control in People with type 2 Diabetes," *JAMA Network Open* 8, no. 10 (2025): e2539278, https://doi.org/10.1001/jamanetworkopen.2025.39278.

9. H. K. Akturk, "Limitations of 14-Day Continuous Glucose Monitoring Sampling for Assessment of Hypoglycemia and Glycemic Variability in type 1 Diabetes," *Diabetes Technology & Therapeutics* 26, no. 7 (2024): 503–508, https://doi.org/10.1089/dia.2023.0476.

10. M. Martinez, J. Santamarina, A. Pavesi, C. Musso, and G. E. Umpierrez, "Glycemic Variability and Cardiovascular Disease in Patients with type 2 Diabetes," *BMJ Open Diabetes Research & Care* 9, no. 1 (2021): e002032, https://doi.org/10.1136/bmjdrc-2020-002032.

11. D. C. Klonoff, M. Gabbay, S. J. Moon, and E. G. Wilmot, "Importance of FDA-Integrated Continuous Glucose Monitors to Ensure Accuracy of Continuous Glucose Monitoring," *Journal of Diabetes Science and Technology* 19, no. 5 (2025): 1392–1399, https://doi.org/10.1177/19322968241250357.

12. V. D. Funtanilla, T. Caliendo, and O. Hilas, "Continuous Glucose Monitoring: A Review of Available Systems," *Pharmacy and Therapeutics* 44 (2019): 550–557.

13. C. Kolluru, R. Gupta, Q. Jiang, et al., "Plasmonic Paper Microneedle Patch for on-Patch Detection of Molecules in Dermal Interstitial Fluid," *ACS Sensors* 4, no. 6 (2019): 1569–1576, https://doi.org/10.1021/acssensors.9b00258.

14. K. M. Saifullah and Z. F. Rad, "Sampling Dermal Interstitial Fluid Using Microneedles: A Review of Recent Developments in Sampling Methods and Microneedle-Based Biosensors," *Advanced Materials Interfaces* 10, no. 10 (2023): 2201763, https://doi.org/10.1002/admi.202201763.

15. S. P. Sullivan, N. Murthy, and M. R. Prausnitz, "Minimally Invasive Protein Delivery with Rapidly Dissolving Polymer Microneedles," *Advanced Materials* 20, no. 5 (2008): 933–938, https://doi.org/10.1002/adma.200701205.

16. B. Q. Tran, P. R. Miller, R. M. Taylor, et al., "Proteomic Characterization of Dermal Interstitial Fluid Extracted Using a Novel Microneedle-Assisted Technique," *Journal of Proteome Research* 17, no. 1 (2018): 479–485, https://doi.org/10.1021/acs.jproteome.7b00642.

17. Z. Wu, Z. Qiao, S. Chen, et al., "Interstitial Fluid-Based Wearable Biosensors for Minimally Invasive Healthcare and Biomedical Applications," *Communications Materials* 5, no. 1 (2024): 33, https://doi.org/10.1038/s43246-024-00468-6.

18. F. Ribet, A. Bendes, C. Fredolini, et al., "Microneedle Patch for Painless Intradermal Collection of Interstitial Fluid Enabling Multianalyte Measurement of Small Molecules, SARS-CoV-2 Antibodies, and Protein Profiling," *Advanced Healthcare Materials* 12, no. 13 (2023): 2202564, https://doi.org/10.1002/adhm.202202564.

19. S. Brown, P. N. Zambrana, X. Ge, et al., "Minimally Invasive Technique for Measuring Transdermal Glucose with a Fluorescent Biosensor," *Analytical and Bioanalytical Chemistry* 410, no. 27 (2018): 7249–7260, https://doi.org/10.1007/s00216-018-1336-8.

20. Y. Wang, Y. Wu, and Y. Lei, "Microneedle-Based Glucose Monitoring: A Review From Sampling Methods to Wearable Biosensors," *Biomaterials Science* 11, no. 17 (2023): 5727–5757, https://doi.org/10.1039/D3BM00409K.

21. D. Kulkarni, D. Gadade, N. Chapaitkar, et al., "Polymeric Microneedles: An Emerging Paradigm for Advanced Biomedical Applications," *Scientia Pharmaceutica* 91, no. 2 (2023): 27, https://doi.org/10.3390/scipharm91020027.

22. B. Darmau, M. Sacchi, I. Texier, and A. J. Gross, "Self-Extracting Dextran-Based Hydrogel Microneedle Arrays," *Advanced Healthcare Materials* 14, no. 2 (2025): 2403209, https://doi.org/10.1002/adhm.202403209.

23. C. M. Wong, K. H. Wong, and X. D. Chen, "Glucose Oxidase: Natural Occurrence, Function, Properties and Industrial Applications," *Applied Microbiology and Biotechnology* 78 (2008): 927–938, https://doi.org/10.1007/s00253-008-1407-4.

24. J. R. Windmiller, G. Valdés-Ramírez, N. Zhou, et al., "Bicomponent Microneedle Array Biosensor for Minimally-Invasive Glutamate Monitoring," *Electroanalysis* 23, no. 10 (2011): 2302–2309, https://doi.org/10.1002/elan.201100361.

25. J. Trzebinski, S. Sharma, A. R. B. Moniz, K. Michelakis, Y. Zhang, and A. E. G. Cass, "Microfluidic Device to Investigate Factors Affecting Performance in Biosensors Designed for Transdermal Applications," *Lab on a Chip* 12, no. 2 (2012): 348–352, https://doi.org/10.1039/C1LC20885C.

26. G. Valdés-Ramírez, Y. C. Li, J. Kim, et al., "Microneedle-Based Self-Powered Glucose Sensor," *Electrochemistry Communications* 47 (2014): 58–62, https://doi.org/10.1016/j.elecom.2014.07.014.

27. M. A. Invernale, B. C. Tang, R. L. York, L. Le, D. Y. Hou, and D. G. Anderson, "Microneedle Electrodes toward an Amperometric Glucose-Sensing Smart Patch," *Advanced Healthcare Materials* 3 (2013): 338–342, https://doi.org/10.1002/adhm.201300142.

28. D. Chen, C. Wang, W. Chen, Y. Chen, and J. X. Zhang, "PVDF-Nafion Nanomembranes Coated Microneedles for In Vivo Transcutaneous Implantable Glucose Sensing," *Biosensors and Bioelectronics* 74 (2015): 1047–1052, https://doi.org/10.1016/j.bios.2015.07.036.

29. J. Ju, L. Li, S. Regmi, X. Zhang, and S. Tang, "Microneedle-Based Glucose Sensor Platform: From Vitro to Wearable Point-of-Care Testing Systems," *Biosensors* 12, no. 8 (2022): 606, https://doi.org/10.3390/bios12080606.

30. P. Bollella, S. Sharma, A. E. Cass, F. Tasca, and R. Antiochia, "Minimally Invasive Glucose Monitoring Using a Highly Porous Gold Microneedles-Based Biosensor: Characterization and Application in Artificial Interstitial Fluid," *Catalysts* 9, no. 7 (2019): 580, https://doi.org/10.3390/catal9070580.

31. K. B. Kim, W. C. Lee, C. H. Cho, D. S. Park, S. J. Cho, and Y. B. Shim, "Continuous Glucose Monitoring Using a Microneedle Array Sensor Coupled with a Wireless Signal Transmitter," *Sensors and Actuators B: Chemical* 281 (2019): 14–21, https://doi.org/10.1016/j.snb.2018.10.081.

32. B. L. Zhang, Y. Yang, Z. Q. Zhao, and X. D. Guo, "A Gold Nanoparticles Deposited Polymer Microneedle Enzymatic Biosensor for Glucose Sensing," *Electrochimica Acta* 358 (2020): 136917, https://doi.org/10.1016/j.electacta.2020.136917.

33. L. Zhao, Z. Wen, F. Jiang, Z. Zheng, and S. Lu, "Silk/Polyols/GOD Microneedle Based Electrochemical Biosensor for Continuous Glucose

26884062, 2026, 5, Downloaded from https://onlinelibrary.wiley.com/doi/10.1002/sstr.70437 by Chung-Ang Library - Chung-Ang University , Wiley Online Library on [07/06/2026]. See the Terms and Conditions (https://onlinelibrary.wiley.com/terms-and-conditions) on Wiley Online Library for rules of use; OA articles are governed by the applicable Creative Commons License

Monitoring," *RSC Advances* 10, no. 11 (2020): 6163–6171, https://doi.org/10.1039/C9RA10374K.

34. Y. Zeng, H. Zhou, J. Ding, and W. Zhou, "Cell Membrane Inspired Nano-Shell Enabling Long-Acting Glucose Oxidase for Melanoma Starvation Therapy via Microneedles-Based Percutaneous Delivery," *Theranostics* 11, no. 17 (2021): 8270, https://doi.org/10.7150/thno.60758.

35. M. Sang, M. Cho, S. Lim, et al., "Fluorescent-Based Biodegradable Microneedle Sensor Array for Tether-Free Continuous Glucose Monitoring with Smartphone Application," *Science Advances* 9, no. 22 (2023): eadh1765, https://doi.org/10.1126/sciadv.adh1765.

36. H. Lee, S. S. Reginald, J. S. Sravan, M. Lee, and I. S. Chang, "Advanced Strategies for Enzyme–electrode Interfacing in Bioelectrocatalytic Systems," *Trends in Biotechnology* 43, no. 6 (2025): 1328–1355, https://doi.org/10.1016/j.tibtech.2024.11.015.

37. N. Kalita, S. Gogoi, S. D. Minteer, and P. Goswami, "Advances in Bioelectrode Design for Developing Electrochemical Biosensors," *ACS Measurement Science Au* 3, no. 6 (2023): 404–433, https://doi.org/10.1021/acsmeasuresciau.3c00034.

38. S. Yu and N. V. Myung, "Recent Advances in the Direct Electron Transfer-Enabled Enzymatic Fuel Cells," *Frontiers in Chemistry* 8 (2021): 620153, https://doi.org/10.3389/fchem.2020.620153.

39. T. Saha, R. Del Caño, K. Mahato, et al., "Wearable Electrochemical Glucose Sensors in Diabetes Management: A Comprehensive Review," *Chemical Reviews* 123, no. 12 (2023): 7854–7889, https://doi.org/10.1021/acs.chemrev.3c00078.

40. M. Adeel, M. M. Rahman, I. Caligiuri, V. Canzonieri, F. Rizzolio, and S. Daniele, "Recent Advances of Electrochemical and Optical Enzyme-Free Glucose Sensors Operating at Physiological Conditions," *Biosensors and Bioelectronics* 165 (2020): 112331, https://doi.org/10.1016/j.bios.2020.112331.

41. M. Adeel, K. Asif, M. M. Rahman, S. Daniele, V. Canzonieri, and F. Rizzolio, "Glucose Detection Devices and Methods Based on Metal–organic Frameworks and Related Materials," *Advanced Functional Materials* 31, no. 52 (2021): 2106023, https://doi.org/10.1002/adfm.202106023.

42. X. Wen, X. Yang, Z. Ge, et al., "Self-Powered Optical Fiber Biosensor Integrated with Enzymes for Non-Invasive Glucose Sensing," *Biosensors and Bioelectronics* 253 (2024): 116191, https://doi.org/10.1016/j.bios.2024.116191.

43. N. Li, N. Eedugurala, D. S. Leem, J. D. Azoulay, and T. N. Ng, "Organic Upconversion Imagers," *Advanced Functional Materials* 31, no. 16 (2021): 2100565, https://doi.org/10.1002/adfm.202100565.

44. F. Hong, P. Qiu, Y. Wang, et al., "Chitosan-Based Hydrogels: From Preparation to Applications, a Review," *Food Chemistry: X* 21 (2024): 101095, https://doi.org/10.1016/j.fochx.2023.101095.

45. S. P. Sullivan, D. G. Koutsonanos, M. del Pilar Martin, et al., "Dissolving Polymer Microneedle Patches for Influenza Vaccination," *Nature Medicine* 16, no. 8 (2010): 915–920, https://doi.org/10.1038/nm.2182.

46. P. Makvandi, M. Kirkby, A. R. J. Hutton, et al., "Engineering Microneedle Patches for Improved Penetration: Analysis, Skin Models and Factors Affecting Needle Insertion," *Nano-Micro Letters* 13, no. 1 (2021): 93, https://doi.org/10.1007/s40820-021-00611-9.

47. American Diabetes Association, "Standards of Medical Care in Diabetes—2009," *Diabetes Care* 32, no. Supplement_1 (2009): S13–S61, https://doi.org/10.2337/dc09-S013.

48. S. H. Tawakey, M. Mansour, A. Soltan, and A. I. Salim, "Early Detection of Hypo/Hyperglycemia Using a Microneedle Electrode Array-Based Biosensor for Glucose Ultrasensitive Monitoring in Interstitial Fluid," *Lab on a Chip* 24, no. 16 (2024): 3958–3972, https://doi.org/10.1039/D4LC00365A.

49. Q. Li, X. Li, J. Wang, et al., "Diagnosis and Treatment for Hyperuricemia and Gout: A Systematic Review of Clinical Practice Guidelines and Consensus Statements," *BMJ Open* 9 (2019): e026677, https://doi.org/10.1136/bmjopen-2018-026677.

50. G. Ye, C. Liu, X. Zheng, et al., "The Effectiveness and Safety of Specific Dietary Supplements in Modulating Uric Acid Levels, Oxidative Stress, and Lipid Metabolism in Patients: A Network Meta-Analysis of 13 interventions," *Nutrition & Metabolism* 22, no. 1 (2025): 80, https://doi.org/10.1186/s12986-025-00977-2.

51. W. H. Organization, "Definition and Diagnosis of Diabetes Mellitus and Intermediate Hyperglycaemia: Report of a WHO/IDF Consultation," (2006), https://iris.who.int/handle/10665/43588.

52. D. P. Sonne and B. Hemmingsen, "Comment on American Diabetes Association. Standards of Medical Care in Diabetes—2017," *Diabetes Care* 40, no. 7 (2017): e92–e93, https://doi.org/10.2337/dc17-0299.

53. A. J. F. King, M. R. Kennard, and M. Nandi, "*Animal Models of Diabetes Methods and Protocols*" (Springer, 2020), 225–239.

54. O. A. Monteiro Jr and C. Airoldi, "Some Studies of Crosslinking Chitosan–glutaraldehyde Interaction in a Homogeneous System," *International Journal of Biological Macromolecules* 26, no. 2–3 (1999): 119–128, https://doi.org/10.1016/S0141-8130(99)00068-9.

55. N. Sharmin, J. T. Rosnes, L. Prabhu, U. Böcker, and M. Sivertsvik, "Effect of Citric Acid Cross Linking on the Mechanical, Rheological and Barrier Properties of Chitosan," *Molecules* 27, no. 16 (2022): 5118, https://doi.org/10.3390/molecules27165118.

56. H. Chang, M. Zheng, X. Yu, et al., "A Swellable Microneedle Patch to Rapidly Extract Skin Interstitial Fluid for Timely Metabolic Analysis," *Advanced Materials* 29, no. 37 (2017): 1702243, https://doi.org/10.1002/adma.201702243.

Supporting Information

Additional supporting information can be found online in the Supporting Information section.

26884062, 2026, 5, Downloaded from https://onlinelibrary.wiley.com/doi/10.1002/sstr.70437 by Chung-Ang Library - Chung-Ang University , Wiley Online Library on [07/06/2026]. See the Terms and Conditions (https://onlinelibrary.wiley.com/terms-and-conditions) on Wiley Online Library for rules of use; OA articles are governed by the applicable Creative Commons License